Comparison of Adaptive Control Laws on a Satellite Attitude Control Benchmark

Yoni Lahana, Mauro Mancini, Dimitri Peaucelle, Elisa Capello, Hélène Evain

Comparison of Adaptive Control Laws on a Satellite Attitude Control Benchmark*

Yoni Lahana[1], Mauro Mancini[2], Dimitri Peaucelle[1], Elisa Capello[2,3] and Hélène Evain[4]

***Abstract*— The CNES satellite DEMETER is taken as a Benchmark to test several control laws. The original control strategy for this mission was to switch between two different control laws according to the pointing error. This switching control made its proof on this mission, but it induces some unwanted behaviour such as oscillations in the control torque at the appearance of the switch and long time responses. In this work, we compare the switching control with continuous adaptive control laws that avoid discontinuities, allow a wider range of initial conditions, and have faster convergence. Three adaptive control laws are described and compared: (i) the DEMETER switching control, (ii) a robust adaptive control where gain evolution is driven by the attitude pointing error, and (iii) a sliding mode control with an adaptive sliding surface. The obtained closed-loop performances are illustrated in small and large pointing error situations.**

I. INTRODUCTION

Attitude control of space vehicles such as satellites is a widely studied problem. It comprises several challenges. One is related to the geometry of rotations in 3-dimensional space [1]. This challenge is particularly stringent for high amplitude maneuvers for which the non-linear nature of the dynamics with multiple equilibria cannot be neglected. Solutions such as those provided by [2] enable global stability, and as described for example in [3], non-linearity compensation enables to simplify the challenge as the stabilization of an almost linear plant. Such results assume the satellite to be a rigid body which is reasonable for large variations of the attitude but are no more appropriate when considering dynamics close to the equilibrium. This is the case for the DEMETER satellite that we use as a benchmark in this paper. As described in [4], the DEMETER mission aimed at measuring transient very-low-frequency electromagnetic phenomena and for that the satellite comprised three long antennas whose (uncertain) flexible modes could not be neglected when considering the very accurate attitude pointing requirements. Robust H_∞/H_2 performance results [5] were applied to obtain high-quality control at low pointing errors as reported in [6]. A third challenge for attitude control is to consider the intermediate situation when the geometry related non-linearities are not stringent but the high-quality aggressive control for low pointing error is not appropriate because of actuators' limitations. One possibility is to have a control law dedicated to such transients. Another solution adopted by CNES is to have an automatic modification of a few control parameters to cope with non-negligible deviations from the small pointing error situation, but has the drawback to generate discontinuities in the control input and gives long time responses. The aim of this paper is to compare the switching strategy that was implemented on DEMETER with alternative adaptive methods.

Adaptive control strategies classically aim for updating control parameters facing complications such as external disturbances or parametric uncertainties. To this end, the indirect adaptive controllers are composed of online estimators of the unknown complications, and adaptation is done based on these estimates [7], while direct adaptive controllers involve an automatic tuning of the parameters based on measurements only. In the paper, we adopt such direct adaptive schemes. More precisely we consider adaptive gains that are tuned by differential equations as in the passivity-based adaptive control literature [8], [9], [10]. Although the adaptation algorithms are very similar, the automatic tuning adopted in the present paper is not ruled by passivity (hence high gain) considerations. On the contrary, following the results already successfully tested in [11], the adaptation strategy enables a mitigation between nominal gain and low gain control, thus avoiding saturation in actuators. This saturation avoidance adaptive rule is applied to the gains involved in the existing switching strategy and to the parameters of a sliding mode controller.

Sliding Mode Control (SMC) theory is a nonlinear control technique with remarkable properties of precision and robustness, which allow a n^{th}-order non-linear system with l inputs to be replaced by an equivalent $n-l$ order problem [12]. In this work, we consider the classical First Order Sliding Mode (FOSM) algorithm, whose design consists in two steps. First, a sliding variable is defined as a function of the states of the system. The sliding surface, *i.e.* the region where the sliding variable is null, is chosen such that trajectories have appropriate stable properties thus guaranteeing the error converges to zero when on the sliding surface (*sliding phase*) [13]. The second step is the design of a discontinuous control law that enforces the system's trajectories to reach the sliding surface in finite time and stay there (*reaching phase*) [14]. It is well known that chattering is the most critical problem of the FOSM algorithm [15], in this work we use the boundary layer SMC [16] to avoid high-frequency oscillations in the command line. Classical FOSM has a constant linear sliding surface, but several strategies for time-

*Work supported by CNES and Région Occitanie, France

[1] LAAS-CNRS, Université de Toulouse, CNRS, Toulouse, France {yoni.lahana, peaucelle}@laas.fr

[2] Politecnico di Torino, Torino, Italy {mauro.mancini, elisa.capello}@polito.it

[3] Institute of Electronics, Computer and Telecommunication Engineering National Research Council of Italy (CNR-IEIIT)

[4] CNES, Toulouse, France helene.evain@cnes.fr

varying sliding surfaces have been proposed and collected in [17] and [18]. These include the usage of predefined time polynomials or fuzzy logic. In the first case, the movement of the sliding surface is merely a function of time and is not adjusted according to the states of the dynamic system. On the other side, fuzzy logic allows to move the sliding surface according to the states of the system but requires the definition of fuzzy sets, input and output decision rules, and defuzzification methods. Here, we propose the usage of a modified FOSM algorithm with a novel direct adaptive law to rotate the linear sliding surface in real-time. This strategy offers the main advantage of requiring only a numerical integration to automatically update the position of the sliding surface based on the states of the system. The details and stability analysis of the new control algorithm are discussed in [19]. The adaptation of the sliding surface allows to reduce the aggressive reaching phase before sliding, thus limiting the saturation of actuators and providing an appropriate solution for the attitude control problem.

The outline of the paper is as follows. First, we recall briefly the attitude control problem for DEMETER as formalized by the CNES engineers. In section 3 we describe the different adaptive and non-adaptive control laws to be compared. Section 4 is then devoted to the exposure of the comparison results in realistic simulations.

II. DEMETER

In this paper, we focus our work on the control of the attitude of the microsatellite DEMETER, the first of the CNES' Myriade series of microsatellites, which was launched in 2004 in Low-Earth Orbit. It was designed to analyze the electromagnetic environment of the Earth [20].

A. Dynamics of the satellite

For the purpose of this work, the CNES provided a benchmark based on [4] and [6] including the simulation of the dynamic and kinematic of the microsatellite, its actuators, the measure of its angular position, the estimation of its angular velocity and the control of its attitude. The Attitude and Orbit Control System (AOCS) of DEMETER includes four different modes. However this paper is only focusing on the normal mode, where the only available actuators are the reaction wheels (one per axis), and magnetotorquers used to desaturate the wheels. The measure of the attitude is provided by a star tracker and the angular velocity is estimated from the attitude. Based on [21], we can write the simplified model of the attitude dynamics and kinematics as

$$\begin{aligned} \dot{h}_{\text{tot}} &= J\dot{\omega} + \dot{h}_{\text{rw}} = T_d \\ \dot{h}_{\text{rw}} &= u = -K_p\theta - K_d\omega \end{aligned} \tag{1}$$

where h_{tot} is the total angular momentum of the spacecraft, h_{rw} the angular momentum of the reaction wheels, J is the inertia, θ is the dynamic attitude error expressed in cardan angles, ω is the angular velocity error, and T_d a disturbance torque induced by external forces. The DEMETER control law is composed of two blocks in series. The first one is a simple diagonal proportional derivative designed for the linearized model (1) of the type $u = -K_p\theta - K_d\omega$. The second block is a high-order linear time-invariant controller designed with H_2/H_∞ optimization assuming the Proportional-Derivative (PD) controller is given and including in the model many complications such as the flexible modes and the reaction wheels. This design is described in [6], and the model of the reaction wheels can be found in [4]. This design allows very accurate tracking performance for small pointing errors.

B. Control objectives

The control objectives of the mission DEMETER are detailed in [4]. For this work, we considered the main requirements:

1) Pointing accuracy should be less than 6.98×10^{-4} rad ($= 0.04°$)
2) Avoidance of reaction wheels' angular rate ($\omega_{\text{rw max}} = 293$ rad/s) and torque ($C_{\text{rw max}} = 0.005$ Nm) saturation

The first of the two items shall be achieved if the control law mimics the (PD, stabilizing filter) structure at small pointing errors. The second criterion needs to diminish appropriately the control efforts when the pointing error is large.

III. CONTROL LAWS

The adopted strategy is to keep in the loop the stabilizing filters and to replace the static PD controller with advanced versions of it that are ultimately equivalent to the PD control at small pointing errors. To keep it simple, all controllers keep the diagonal structure of the initial PD control. The index $j = \{X, Y, Z\}$ indicates the satellite's main axes.

A. Switching PD

The control law developed by CNES and implemented on the spacecraft's onboard computer [4] is a switching control law. It switches according to the pointing error as follows:

$$|\theta_j| \geq \theta_{tj} \Rightarrow u_j(t) = -b_j \textbf{sign}(\theta_j(t)) - \omega_j(t) \tag{2a}$$

$$|\theta_j| < \theta_{tj} \Rightarrow u_j(t) = -K_{pj}\theta_j(t) - K_{dj}\omega_j(t) \tag{2b}$$

The numerical values of the parameters can be found in [4]. K_{pj} and K_{dj} are the static PD gains chosen for the linearized model (1). The switching value θ_{tj} is given from engineering considerations and the speed bias b_j is such that $K_{p_j}\theta_{tj} = K_{dj}b_j$ in order to minimize discontinuities when $u_j(t) \simeq 0$.

B. Adaptive PD

A continuous adaptive version of the PD-controller has been proposed in [22] and tested in flight on the PICARD satellite [11]. The control law is exactly that of the switching PD controller

$$u_j(t) = -K_{\theta j}(t)\theta_j(t) - K_{\omega j}(t)\omega_j(t) \tag{3}$$

with the difference that the gains evolve in time according to differential equations:

$$\dot{K}_{\theta j}(t) = \mathbf{Proj}_{\mathcal{K}_{\theta j}}\left(-G_{\theta j}\theta_j^2(t) - c_{\theta j}(K_{\theta j}(t) - K_{pj})\right) \tag{4a}$$

$$\dot{K}_{\omega j}(t) = \mathbf{Proj}_{\mathcal{K}_{\omega j}}\left(-G_{\omega j}\theta_j^2(t) - c_{\omega_j}(K_{\omega j}(t) - K_{dj})\right) \tag{4b}$$

In these equations the $\mathbf{Proj}_{\mathcal{K}}$ is a projection operator that guarantees that the gains are at all times bounded $K(t) \in \mathcal{K}$. In practice, these differential equations are coded as saturated integrators. The sets are chosen as follows $\mathcal{K}_{\theta j} = [\ 0.02K_{pj}\ ,\ K_{pj}\ ]$ and $\mathcal{K}_{\omega j} = [\ 1\ ,\ K_{dj}\ ]$, where K_{pj} and K_{dj} are the same PD gains as previously. $K_{\theta j}$ is hence allowed to be at most equal to the proportional gain of the PD controller and to decrease close to zero down to 2% of its maximal value. $K_{\omega j}$ is allowed to vary continuously between the two values in the switching control law. The $G_{\theta j} > 0$ gain is designed to decrease the proportional gain $K_{\theta j}(t)$ if the pointing error θ_j is large. The same reasoning applies to the $G_{\omega j}$ gain. These adaptation terms aim at avoiding actuator saturation and lead to a controller that behaves as (2a) for large pointing errors. The $c_{\theta j} > 0$ and $c_{\omega j} > 0$ damping coefficients drive the control gains to the PD values K_{pj} and K_{dj} when pointing errors are small. Having in mind the value θ_{tj} that is used by the engineers to distinguish the large and small pointing errors the following constraint is considered in the design of the parameters:

$$G_{\theta j}\theta_{tj}^2 \simeq c_{\theta j}(K_{pj} - 0.02K_{pj}) \tag{5}$$

and a similar constraint is considered for the gains in (4b). $G_{\theta j}$ and $G_{\omega j}$ values are chosen reasonably high but not too high in order to be implementable, that is, if $\overline{\theta}_j$ is an upper bound on the pointing error and T_s is the sampling time, then one has to guarantee

$$\frac{1}{T_s}(K_{pj} - 0.02K_{pj}) \geq G_{\theta j}\overline{\theta}_j^2. \tag{6}$$

A similar constraint is considered for the gains in (4b).

As described, the design of the adaptive law is done in the present case based on engineering considerations. It is not based on any formal condition that would ensure stability or other properties (the same holds for the switching control law). But proofs of stability may nevertheless be achieved based on Lyapunov certificates and solved numerically by LMI solvers. As described in [23], [24] the matrix inequality conditions may also help in tuning the control parameters.

C. First order sliding mode controller

Before considering adaptive sliding mode control, let us formulate the classical sliding mode controller that may replace the switching PD controller. Such control law is of the type $u_j(t) = -K_j\mathbf{sign}(\sigma_j(t))$ where $\sigma_j(t) \equiv 0$ is the sliding surface. It is well known that such controller suffers from high-frequency switching near the sliding surface (and hence at the equilibrium point) as chattering occurs due to discontinuity of signum function. To avoid chattering, a boundary layer of width S_j is introduced:

$$u_j(t) = -K_j\mathbf{sat}_{S_j}(\sigma_j(t)) \tag{7}$$

where the saturation function is:

$$\mathbf{sat}_S(\sigma) = \begin{cases} \mathbf{sign}(\sigma) & \text{if } |\sigma| \geq S \\ \sigma/S & \text{if } |\sigma| < S \end{cases} \tag{8}$$

The sliding surface is chosen to be:

$$\sigma_j(t) = \omega_j(t) + \lambda_j\theta_j(t), \quad \lambda_j \in \mathbb{R}^+ \tag{9}$$

and is such that when $\sigma_j(t) \simeq 0$ (sliding phase) the system behaves as a stable first-order plant $\omega_j(t) = \dot{\theta}_j(t) \simeq -\lambda_j\theta_j(t)$.

Close to the origin the actual control is $u_j(t) = -\frac{K_j}{S_j}\sigma_j(t) = -\frac{K_j}{S_j}(\omega_j(t) + \lambda_j\theta_j(t))$. It coincides with the static PD controller (2b) for the choice of $K_j\lambda_j/S_j = K_{pj}$ and $K_j/S_j = K_{dj}$. Parameters of the sliding mode controller are selected to satisfy this property in order to recover the performances of the switching PD control at low pointing error. K_j is chosen as a trade-off between good disturbance rejection (high gain) and saturation avoidance (low gain).

D. First order sliding mode controller with adaptive sliding surface

The non-adaptive sliding mode control exposed upper behaves exactly the same as the static PD control when close to the sliding surface. It therefore has the same drawbacks as this controller in terms of saturation of the actuators when far from zero pointing error. Moreover, the saturation may prevent the control from actually reaching the sliding surface. Inspired by the adaptive control strategy, the proposed adaptive sliding mode control is as upper (7) but with an equivalent proportional gain $K_j\lambda_{aj}(t)/S_j$ that is decreased when the pointing error is large. The adaptive sliding surface is:

$$\sigma_j(t) = \omega_j(t) + \lambda_{aj}(t)\theta_j(t) \tag{10}$$

where the parameter evolves in time according to

$$\dot{\lambda}_{aj}(t) = \mathbf{Proj}_{\Lambda_j}\left(-G_j\theta_j^2(t) - c_j(\lambda_{aj}(t) - \lambda_j)\right) \tag{11}$$

The projection operator guarantees the slope of the sliding surface to remain in $\Lambda_j = [\ 0.05\lambda_j\ ,\ \lambda_j\ ]$. At most the slope is that of the non-adaptive controller but it is allowed to have positive values close to zero (down to 5% of its maximal value).

The adaptive sliding mode control has the following characteristics. Only the sketch of the Lyapunov-based proofs are given for limited space reasons.

1) As long as $G_j\theta_j^2(t) > c_j(\lambda_j - 0.05\lambda_j) + \alpha_1$ the function $v_{1j} = (\lambda_{aj} - 0.05\lambda_j)^2$ is such that $\dot{v}_{1j} < -\alpha_1 v_{1j}^{1/2}$. It proves finite-time convergence of $\lambda_{aj}(t)$ to its minimal value $0.05\lambda_j$ at large pointing errors.
2) The function $v_{2j} = \sigma_j^2$ is such that $\dot{v}_{2j} < (d_j - \frac{K_j}{J_j})v_{2j}^{1/2}$ when $v_{2j} > {S_j}^2$ and where d_j are terms due to non-linearities, disturbances, the angular rate ω_j and $\dot{\lambda}_j$.

TABLE I: Parameters for given K_{pj} and K_{dj}

Control law	Parameters
Switching PD	θ_{tj}, b_j
Adaptive PD	$G_{\theta j}$, $G_{\omega j}$, $c_{\theta j}$, $c_{\omega j}$
Classical sliding mode	K_j, S_j, λ_j
Adaptive sliding mode	K_j, S_j, λ_j, G_j, c_j

TABLE II: Numerical values of the parameters

$\theta_t = 10^{-3}\begin{pmatrix}5.2 & 8.7 & 2.5\end{pmatrix}$
$b = 10^{-4}\begin{pmatrix}2.618 & 4.363 & 2.618\end{pmatrix}$
$G_\theta = \begin{pmatrix}39.92 & 39.92 & 39.92\end{pmatrix}$
$G_\omega = \begin{pmatrix}798.4 & 798.4 & 798.4\end{pmatrix}$
$c_\theta = c_\omega = \begin{pmatrix}1.0966 & 3.0462 & 1.0966\end{pmatrix}$
$G = 10^{-2}\begin{pmatrix}-4.54 & -2.72 & -4.54\end{pmatrix}$

$K_p = \begin{pmatrix}0.1 & 0.1 & 0.1\end{pmatrix}$
$K_d = \begin{pmatrix}2 & 2 & 2\end{pmatrix}$
$K = 10^{-4}\begin{pmatrix}5 & 5 & 5\end{pmatrix}$
$S = 10^{-4}\begin{pmatrix}2.5 & 2.5 & 2.5\end{pmatrix}$
$\lambda = \begin{pmatrix}0.05 & 0.05 & 0.05\end{pmatrix}$
$c = 10^{-3}\begin{pmatrix}5 & 5 & 5\end{pmatrix}$

Under some mild assumptions, one can conclude about finite-time convergence of $\sigma_j(t)$ to the set $\{|\sigma_j| \leq S_j\}$ for large enough values of K_j. The smaller S_j is, the smaller is this sliding boundary layer.

3) The function $v_{3j} = \theta_j^2$ is such that $\dot{v}_{3j} < -0.1\lambda_j v_{3j} + 2\theta_j\sigma_j$. It allows to conclude about the asymptotic convergence of $\theta_j(t)$ to a neighborhood of zero once $\sigma_j(t)$ has reached the small sliding boundary layer.

4) The function $v_{4j} = (\lambda_{aj} - \lambda_j)^2$ is such that $\dot{v}_{4j} < -c_j v_{4j} + G_j\theta_j^2(\lambda_j - 0.05\lambda_j)$. It proves asymptotic convergence of $\lambda_{aj}(t)$ to λ_j when the pointing error $\theta_j(t)$ is small.

1) is a phase where the sliding surface rotates rapidly in presence of a large pointing error thus helping the avoidance of actuator saturation. 2) is the classical reaching phase of sliding mode control. 3) is the sliding phase. 4) ensures high gain control when close to zero pointing error.

E. Overview of the controllers

All controllers are variations on the original switching PD controller and introduce a limited number of additional parameters (summarized in Table I). The tuning of these parameters, as described, is rather easy based on engineering considerations.

Concerning onboard implementation, the adaptive control laws are slightly more involved than the switching controller because they include first-order differential equations. Compared to the high-order 'stabilizing filters' this does not bring much complication to the implementation.

Table II gives the values of the parameters used in all our simulations. The format is such that $K_p = \begin{pmatrix}K_{px} & K_{py} & K_{pz}\end{pmatrix}$.

IV. SIMULATION RESULTS

All tests are done on a non-linear simulator of the DEMETER satellite provided by CNES and described in [4]. It simulates in particular the dynamics of the rigid satellite and the reaction wheels including the saturations in velocity and torque. The external perturbations are modelled and compensated partially by magnetotorquers. The goal of these simulations is to challenge the control laws with respect to various situations. Only part of these simulations are described in the following for space limitation reasons. The selected simulations illustrate the main properties of the compared controllers.

A. Behaviour at small pointing errors

For a start, we consider situations when initial conditions are rather close to zero pointing errors but above the attitude threshold θ_{tj}. For the adaptive laws, the responses depend on the initial conditions of the differential equation driving the adaptation. To cope with extreme situations the simulations are started with adaptive parameters at the lower bounds of the intervals $\mathcal{K}_\theta$, $\mathcal{K}_\omega$ and Λ. Typically such initial conditions are not appropriate for small pointing errors, but gains are expected to converge to the upper bounds of the intervals which correspond to the static PD-control. At the time $t = 2000s$ a jump is made on the system's states (which corresponds to a step input on the reference attitude), without doing any reset of the adaptive gains. The time response is then what can be expected for initial adaptive gains at the other extreme of the admissible intervals. The difference between the two situations illustrates the variety of responses depending on the states of the adaptive laws. In practice, the first part of the simulations corresponds to a behaviour after a reset of the controller, while the second part of the simulation corresponds to a change of reference during operation. Fig. 1 gives the time responses of the attitude in the X-axis. In the first part of the simulation, the adaptive controllers have worse time responses than the non-adaptive ones, because they start from a bad initial guess of the control parameters. In the second part of the simulation, all controllers give approximately the same response which, as expected, is the closed-loop performance with the static PD control. The only controller that gives a slower time-response is the switching PD that has a short initial speed-bias phase (2a).

Simulations are done with non-zero oscillations as external torque perturbations. Fig. 2 provides a zoom on the pointing error in response to these perturbations. As expected, by design the responses are identical for all controllers and all satisfy the pointing accuracy performance.

Fig. 3 illustrates the adaptation of the $K_{\theta x}(t)$ gain that indeed is almost unchanged during the second phase of the simulation. The same behavior is observed for the adaptation of $\lambda_{ax}(t)$.

Fig. 4 shows the control signal delivered by the controllers. The reaching phase of the sliding mode controllers (constant control) is clearly visible. At times $t \in [0\ 5]s$ $\lambda_{ax}(t)$ is small and hence the plant is in the neighborhood of the adaptive sliding surface (no reaching phase). At times $t \in [2000\ 2005]s$ $\lambda_{ax}(t)$ is large and hence the behaviour is the same as the non-adaptive sliding mode controller.

B. Behaviour at large pointing errors

At large pointing errors, the non-adaptive sliding mode controller generates very aggressive saturating inputs on the system thus generating unstable trajectories. Fig. 5 illustrates these instabilities.

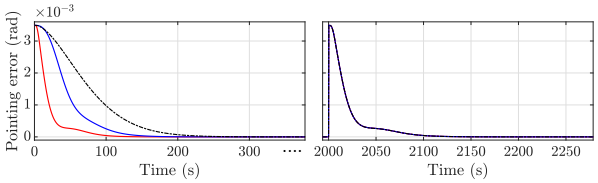

Fig. 1: Attitude in the X-axis with the switching PD (solid red), adaptive PD (solid blue), sliding mode (dashed green), and adaptive sliding mode (dash-dotted black) controllers.

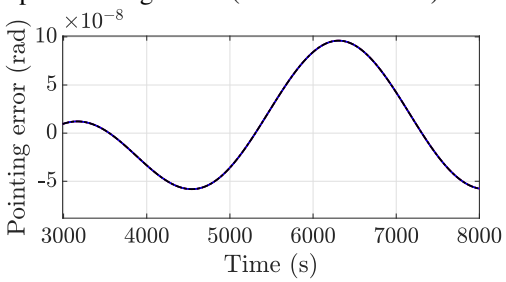

Fig. 2: Zoom of Fig. 1 at steady state, responses to perturbations around the zero pointing error equilibrium.

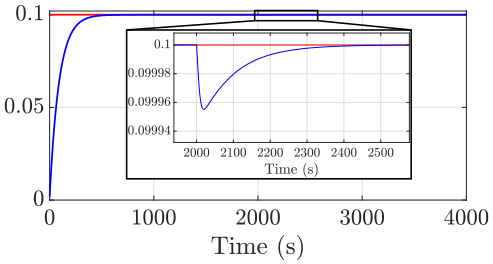

Fig. 3: Constant K_{px} (solid red) and the adaptive $K_{\theta x}(t)$ (solid blue) for the simulation of Fig. 1.

We now concentrate our comparison between the switching PD, the adaptive PD, and the adaptive sliding mode controllers. Fig. 6 illustrates the type of time responses that one gets. The previous scenario is considered. The adaptive controllers provide a convergence comparable to the switching PD.

The Fig. 7 illustrates a discontinuity of the control signal at $t \simeq \{2050s,\ 3050s\}$ due to switch in the CNES controller, phenomenon that is avoided with the continuous adaptive laws. The figure also shows a torque saturation for the adaptive PD during a very short time. This is due to the value of the adaptive gains that are at their maximum value set for small pointing error, thus giving a non-appropriate control input at the occurrence of the jump. This can be avoided if the controller is reset simultaneously with the jump. Although, note on Fig. 8 that the reaction wheel's angular rate does not saturate.

Fig. 8 gives the angular rate of the reaction wheel during the maneuver. By construction, the switching PD provides the smallest peaks on these angular rates. Time histories of the adaptive gains are given in Fig. 9 and 10.

Fig. 11 gives the time response expected for numerous initial pointing errors taken between $\theta_j(0) = [0,\ 2.1]$ rad $(= 120°)$.

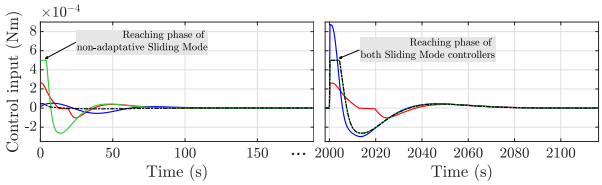

Fig. 4: Control signals delivered by the controllers for the simulation of Fig. 1. Switching PD (solid red), adaptive PD (solid blue), sliding mode (solid green), and adaptive sliding mode (dash-dotted black) controllers

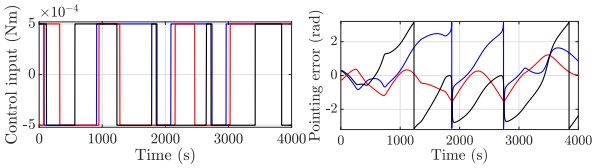

Fig. 5: Pointing error and control input generated for the non-adaptive sliding mode controller with large initial pointing error. Colors are for the X axis (blue), Y axis (red), and Z axis (black).

As shown, the time response for the switching PD grows almost linearly due to (2a) decreasing slowly the attitude error for actuators' limitations. The adaptive controllers give improved time response although, for the adaptive PD, reaction wheels' torque and angular rate saturation occur respectively from $\theta(0) \simeq 0.5$ rad and $\theta(0) \simeq 1.5$ rad.

V. CONCLUSION

The paper provides a comprehensive description of several control laws and their design for the attitude control of the DEMETER satellite benchmark. All controllers have the same properties at close to zero pointing error. Controllers that have no adaption properties are unable to stabilize the plant for large pointing errors. The adaptive controllers achieve this property with very different transients. Although the tuning of the various parameters of the controllers follows a comprehensive rationale we should say that it requires nevertheless some amount of trial and error. Based on the achieved experience, ongoing work is conducted for providing theoretically based conditions to help the design of the adaptive controllers.

REFERENCES

[1] N. Chaturvedi, A. Sanyal, and N. McClamroch, "Rigid-body attitude control," *IEEE Control Systems Magazine*, vol. 31, no. 3, pp. 30–51, 2011.

[2] C. G. Mayhew, R. G. Sanfelice, and A. R. Teel, "Quaternion-based hybrid control for robust global attitude tracking," *IEEE Transactions on Automatic Control*, vol. 56, no. 11, 2011.

[3] T. Conord and D. Peaucelle, "Continuous quaternion based almost global attitude tracking," in *IEEE Conference on Control Technology and Applications (CCTA 2021)*, San Diego, United States, Aug. 2021.

[4] C. Pittet and D. Arzelier, "Demeter: A benchmark for robust analysis and control of the attitude of flexible micro satellites," *IFAC Proceedings Volumes*, vol. 39, no. 9, pp. 661–666, 2006.

[5] C. Scherer, P. Gahinet, and M. Chilali, "Multiobjective output-feedback control via LMI optimization," *IEEE Trans. Automatic Control*, vol. 42, no. 7, pp. 896–911, Jul. 1997.

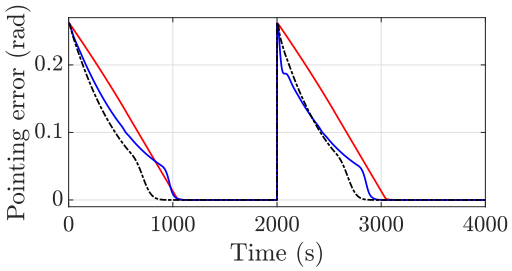

Fig. 6: Attitude in the X-axis with the switching PD (solid red), the adaptive PD (solid blue), the adaptive sliding mode (dash-dotted black) controllers.

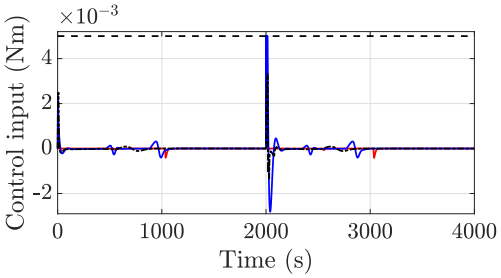

Fig. 7: Control signals delivered by the controllers for the simulation of Fig. 6.

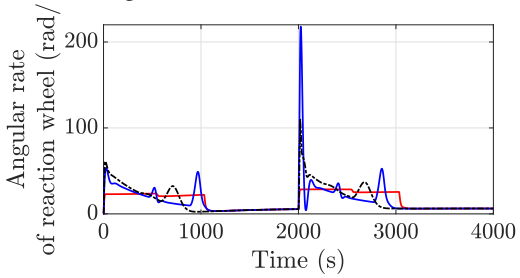

Fig. 8: Angular rate of the reaction wheel (X-axis) for the simulation of Fig. 6.

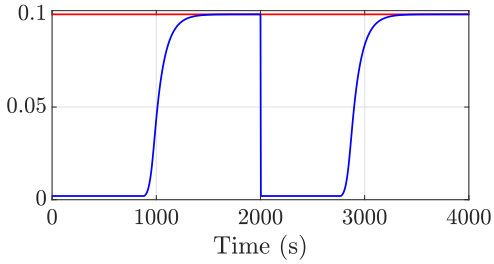

Fig. 9: Constant K_{px} (solid red) and the adaptive $K_{\theta x}(t)$ (solid blue) for the simulation of Fig. 6.

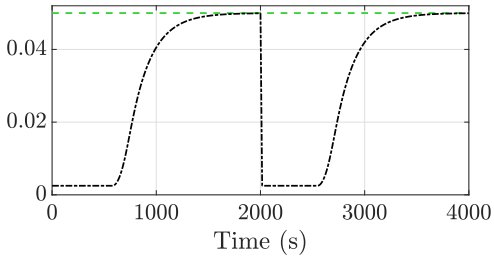

Fig. 10: Constant λ_x (dashed green) and the adaptive $\lambda_{ax}(t)$ (dash-dotted black) for the simulation of Fig. 6.

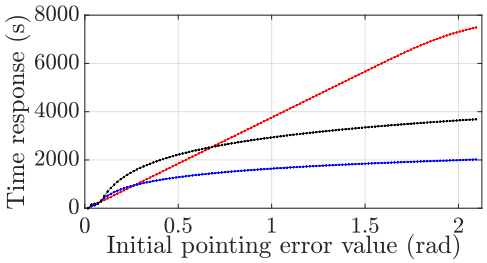

Fig. 11: Time-response with respect to initial pointing error for the switching PD (red), the adaptive PD (blue), and the adaptive sliding mode (black) controllers.

[6] C. Pittet and C. Fallet, "Gyroless attitude control of a flexible microsatellite," in *Conference on Dynamics and Control of Systems and Structures in Space, Cambridge, UK*. Citeseer, 2002.

[7] P. Ioannou and B. Fidan, *Adaptive Control Tutorial*, ser. Advances in Design and Control. SIAM, 2006.

[8] A. Fradkov, "Adaptive stabilization of a linear dynamic plant," *Autom. Remote Contr.*, vol. 35, no. 12, pp. 1960–1966, 1974.

[9] H. Kaufman, I. Barkana, and K. Sobel, *Direct adaptive control algorithms*. New York: Springer, 1998, second Edition.

[10] A. Fradkov, I. Miroshnik, and V. Nikiforov, *Nonlinear and Adaptive Control of Complex Systems*. Dordrekht: Kluwer Academic Publishers, 1999.

[11] C. Pittet, A. Luzi, D. Peaucelle, J.-M. Biannic, and J. Mignot, "In flight results of adaptive attitude control law for a microsatellite," *CEAS Space Journal*, vol. 7, no. 2, pp. 291–302, Dec. 2015.

[12] J.-J. E. Slotine, W. Li *et al.*, *Applied nonlinear control*. Prentice hall Englewood Cliffs, NJ, 1991, vol. 199, no. 1.

[13] Y. Shtessel, C. Edwards, L. Fridman, A. Levant *et al.*, *Sliding mode control and observation*. Springer, 2014, vol. 10.

[14] V. Utkin, "Variable structure systems with sliding modes," *IEEE Transactions on Automatic control*, vol. 22, no. 2, pp. 212–222, 1977.

[15] V. Utkin and H. Lee, "Chattering problem in sliding mode control systems," in *International Workshop on Variable Structure Systems, 2006. VSS'06.*, 2006, pp. 346–350.

[16] J.-J. Slotine and S. S. Sastry, "Tracking control of non-linear systems using sliding surfaces, with application to robot manipulators," *International journal of control*, vol. 38, no. 2, pp. 465–492, 1983.

[17] S. Tokat, M. S. Fadali, and O. Eray, "A classification and overview of sliding mode controller sliding surface design methods," in *Recent Advances in Sliding Modes: From Control to Intelligent Mechatronics*. Springer, 2015, pp. 417–439.

[18] A. Bartoszewicz and A. Nowacka-Leverton, *Introduction*. Berlin, Heidelberg: Springer Berlin Heidelberg, 2009, pp. 1–16. [Online]. Available: https://doi.org/10.1007/978-3-540-92217-9_1

[19] M. Mancini, "Adaptive variable structure control system for attitude spacecraft applications," Ph.D. dissertation, Politecnico di Torino, 2023, available soon.

[20] T. Cussac, M.-A. Clair, P. Ultré-Guerard, F. Buisson, G. Lassalle-Balier, M. Ledu, C. Elisabelar, X. Passot, and N. Rey, "The demeter microsatellite and ground segment," *Planetary and Space Science*, vol. 54, no. 5, pp. 413–427, 2006.

[21] Y. Yang, *Spacecraft Modeling, Attitude Determination, and Control Quaternion-based Approach: Quaternion-Based Approach*. CRC Press, 2019.

[22] A.-R. Luzi, "Commande variante dans le temps pour le contrôle d'attitude de satellites," Ph.D. dissertation, Institut Supérieur de l'Aéronautique et de l'Espace-ISAE, 2014.

[23] A. Luzi, D. Peaucelle, J.-M. Biannic, C. Pittet, and J. Mignot, "Structured adaptive attitude control of a satellite," *Int. J. of Adaptive Control and Signal Processing*, vol. 28, no. 7-8, pp. 664–685, 2014.

[24] D. Peaucelle and H. Leduc, "Adaptive control design with S-variable LMI approach for robustness and L_2 performance," *Int. J. Control*, vol. 93, pp. 194–203, 2020.